A New Fault Detection Method for Single-Phase Auto-Reclosing

L. M. N. de Mattos, M. C. Tavares, *Senior Member, IEEE,* and A. M. P. Mendes

***Abstract*—Single-phase auto-reclosing (SPAR) is among the alternatives for mitigating the many harmful effects that a line-to-ground fault in a transmission line (TL) may cause. This procedure basically consists of opening the compromised phase, waiting a preset time span (dead time), and recomposing the previously isolated phase. In the vast majority of SPAR implementations, the open phase switching proceeds with no guarantee of whether the TL is still faulted. Switching the open phase into a fault might represent a more severe threat to the system than simply disconnecting the TL in the first place. Hence, in an effort to ensure higher levels of operational reliability to SPAR, the present paper offers a new methodology to check the soundness of the open phase during the dead time before its reclosing. First, the method's fundamental concepts are exposed. Second, a huge number of steady-state tests are presented, for which both the system topology and its operative condition were varied. To conclude, the SPAR is simulated in the time-domain with the most critical condition found in the steady-state analysis. The proposed strategy was capable of correctly identifying whether the system was faulted in every performed simulation.**

***Index Terms*—Adaptive Single-Phase Reclosing, Open Phase Voltage Prediction, Unbalanced Power Flow, Alternative Transients Program (ATP), EMTP Simulation.**

I. Introduction

SINGLE-PHASE auto-reclosing (SPAR) may significantly increase the robustness of electric power systems to the most frequent fault type in Extra High Voltage (EHV) and Ultra High Voltage (UHV) transmission lines (TL): line-to-ground (LG) temporary faults - Tables I and II. Briefly, some of the advantages of SPAR are as follows [1]–[6]:

- Greater stability margin in tie-lines compared to three-pole automatic reclosing (TPAR) because it restricts the frequency and amplitude of oscillations between generators;
- Reduced torsional stress in generator shafts given that active power variation (ΔP) and the angle drift ($\Delta\delta$) tend to be smaller than those obtained with TPAR, especially for single circuit interconnections;
- Smaller switching overvoltages compared with TPAR due to the decreased trapped charge in the faulted phase, in contrast to the sound phases. This promotes reduced sustained voltages before the circuit-breaker (CB) reclosing in SPAR compared with TPAR;
- Possibility of maintaining feeding loads at approximately 50-70 % of the pre-fault power flow, which improves continuity rates; and
- Enhanced overall reliability of the electric network in the face of multiple contingencies as a result of keeping the power system stronger in comparison with TPAR.

Table I
FORCED AERIAL TL TRIPPING CAUSED BY ELECTRIC FAULTS IN THE BRAZILIAN INTERCONNECTED POWER SYSTEM (SIN) - YEAR 2016 - CLASSIFIED BY FAULT TYPE [%][7].

Rated voltage [kV]	LLL/G	LLL	LL/G	LL	L/G
750	0.0	4.6	0.0	0.0	95.4
600	0.0	0.0	0.0	0.0	100.0
500	0.0	1.1	1.9	10.7	86.4
440	0.0	2.7	1.4	1.4	94.5
345	0.0	1.1	1.6	3.7	93.6
230	0.1	1.7	3.2	7.7	87.3
All	0.0	1.4	2.4	8.1	88.0

Note: The data from [7] were recalculated to eliminate the original failure statistics motivated by causes other than faults.

Table II
PERCENTAGE OF TEMPORARY FAULTS IN AERIAL TL.

Reference	Temporary [%]	Rated voltage [kV]
[8]	>90	-
[9]	93.1	400
[9]	91.9	220
[9]	93.4	132

Despite the many benefits of SPAR, when this procedure is performed unsuccessfully, it can have more severe impacts on the system than LG faults and the following TL tripping. The success of SPAR may be compromised if it is realized without sufficient dead time to allow the secondary arc to extinguish fully, or when the insulation medium (air) does not recover its dielectric characteristic completely to withstand the switching overvoltages, or simply because the fault is not of a temporary type, being so-called permanent. If the system were designed to address an unsuccessful SPAR, it would lead to a smaller stability margin than when not considering it or when adopting TPAR. Extending the dead time duration would contribute to an increase in the probability of secondary arc extinction, although it is not a perfect solution because it could raise stability concerns, permanent faults remain a threat, and it would subject the electric network to unbalanced operation over longer times. This condition is undesired since

L. M. N. de Mattos is a self-employed consultant in Brazil (e-mail: l@mattos.eng.br).

M. C. Tavares is with the University of Campinas, Brazil (e-mail: ctavares@unicamp.br).

A. M. P. Mendes is with Eletrobras Eletronorte, Brazil (e-mail: anielampm@protonmail.ch).

Manuscript received April 19, 2005; revised August 26, 2015.

This work was partially supported by the research agency FAPESP (2017/20010-1) and CNPq, Brazil.

it can trigger misconfigured protections, impose additional shaft stresses and heating in electrical machinery, and cause malfunctions in other three-phase loads.

Nonetheless, the most complex SPAR-associated issues arise from the dead time length definition and the possibility of switching to a faulted phase. To address these issues, research is being performed on detecting the secondary arc extinction instant and discriminate permanent faults from temporary faults, thus permitting two major gains: decreased the SPAR dead time by accelerating the open phase reclosing when the unfaulted time span is sufficient to deionize the arc channel and blocking SPAR under the condition that the TL remains faulted at the end of the dead time. Due to the importance of the matter, diverse techniques have been proposed to detect secondary arc extinction based on various concepts, which can be roughly split among a few categories such as harmonic content [10]–[17], traveling waves [18], zero sequence active power [19], artificial neural networks [20], PMU [21], and open phase voltage processing [5], [22]–[26].

The objective of the present paper is to introduce the main concepts and the mathematical background of a new method for detecting, in real time, whether the opened phase for SPAR remains faulted before its reclosing. The proposed solution is based on a comparison of the predicted open phase voltage fundamental frequency phasor, computed for the TL sound condition, against the calculated phasor from the actual open phase measurements. In addition, a narrow margin is given to accommodate eventual phasor computations and system parameter errors.

To test the proposed methodology, a massive number of steady-state simulations comprehending variations in several topological and operative parameters, therein being focused on testing the reliability of the presented strategy, are offered. This approach was chosen because it is envisioned to use the fundamental frequency phasors. If the phasors were perfectly estimated, they would show the network forced response only, even under unbalanced operational conditions. Additionally, the most critical configuration, found in the steady-state analysis, is used as the test base for a time-domain simulation of the proposed method along SPAR.

II. Proposed Method

A. Theoretical Basis

The SPAR grants suitable boundary conditions for the use of a three-phase four-port network TL model [27], [28] because both CBs of the faulted phase are open during the dead time. Hence, the currents in those CBs are zero. This fact enables the decoupling of the four-port network inter-terminal dependence precisely in the matrix row that describes the current circulation in the open phase. Assuming that phase A is the faulted one, this condition can be summarized as $I_a^m = I_a^n = 0$, where the superscript and subscript indices describe the associated TL terminal and the phase, respectively.

Consider a four-port network that represents a single-circuit three-phase TL, $[Q_{TL}]$, composed of q_{ij} terms such as:

$$\begin{bmatrix} V_a^m \\ V_b^m \\ V_c^m \\ I_a^m \\ I_b^m \\ I_c^m \end{bmatrix} = \begin{bmatrix} q_{11} & q_{12} & q_{13} & q_{14} & q_{15} & q_{16} \\ q_{21} & q_{22} & q_{23} & q_{24} & q_{25} & q_{26} \\ q_{31} & q_{32} & q_{33} & q_{34} & q_{35} & q_{36} \\ q_{41} & q_{42} & q_{43} & q_{44} & q_{45} & q_{46} \\ q_{51} & q_{52} & q_{53} & q_{54} & q_{55} & q_{56} \\ q_{61} & q_{62} & q_{63} & q_{64} & q_{65} & q_{66} \end{bmatrix} \cdot \begin{bmatrix} V_a^n \\ V_b^n \\ V_c^n \\ I_a^n \\ I_b^n \\ I_c^n \end{bmatrix} \quad (1)$$

Applying the aforementioned boundary conditions to the fourth row of (1), we have:

$$0 = \begin{bmatrix} q_{41} & q_{42} & q_{43} & q_{44} & q_{45} & q_{46} \end{bmatrix} \cdot \begin{bmatrix} V_a^n \\ V_b^n \\ V_c^n \\ 0 \\ I_b^n \\ I_c^n \end{bmatrix} \quad (2)$$

The voltages and currents V_b^n, V_c^n, I_b^n and I_c^n are quantities that are typically acquired in TL terminals for protection schemes and/or accountability. If the TL parameters are also known ($[Q_{TL}]$ matrix), then it is possible to calculate the exact steady-state voltage at the TL open terminal with the following expression:

$$V_a^n = -\frac{1}{q_{41}} \begin{bmatrix} q_{42} & q_{43} & q_{45} & q_{46} \end{bmatrix} \cdot \begin{bmatrix} V_b^n \\ V_c^n \\ I_b^n \\ I_c^n \end{bmatrix} \quad (3)$$

Notwithstanding, when the TL is still faulted, the electric network cannot be solely described by $[Q_{TL}]$ because it does not take the line-to-ground connection into account. Nevertheless, this can be done using a four-port network cascade, therein placing a shunt connection in the faulted phase, as shown in Fig. 1 and (4):

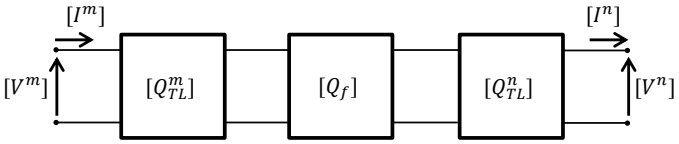

Figure 1. LG fault representation with four-port network cascade.

$$[Q_{TL,f}] = [Q_{TL}^m][Q_f][Q_{TL}^n] \quad (4)$$

where $[Q_{TL}^m]$, $[Q_f]$ and $[Q_{TL}^n]$ are the four-port network modeling the TL section from terminal m up to the fault insertion point, the fault shunt connection conductance and the TL section from the fault point to terminal n, respectively.

Since the unfaulted condition can be also represented by the cascade $[Q_{TL}] = [Q_{TL}^m][Q_{TL}^n]$, the modification caused by the fault insertion can be found using:

$$[\Delta Q_f] = [Q_{TL,f}] - [Q_{TL}^m][Q_{TL}^n] \quad (5)$$

Solving (5) and observing its results, it is possible to describe each element of $[\Delta Q_f]$ as:

$$\delta q_{f,ij}^a = g_f q_{i4}^m q_{1j}^n \quad (6)$$

For faults in phases B and C, we have:

$$\delta q^{b}_{f,ij} = g_f q^{m}_{i5} q^{n}_{2j} \tag{7}$$

$$\delta q^{c}_{f,ij} = g_f q^{m}_{i6} q^{n}_{3j} \tag{8}$$

Analyzing (6), (7) and (8), the most evident fact is that every element of $[\Delta Q_f]$ is multiplied by the scalar fault conductance g_f. That makes sense because once the fault is eliminated, its conductance goes to zero, and its effects in the original TL model must then vanish, resulting in $[Q_{TL}] = [Q_{TL,f}]$.

B. Detecting the Arc Extinction

This paper takes advantage of the above-cited network change between TL terminals, motivated by the fault inception, to propose a new method to detect whether the opened phase for SPAR is in a sound condition before its reclosing step. This is accomplished by comparing the open phase voltage measured phasor against the expected phasor when the TL is under unfaulted conditions. The sound open phase phasor should be calculated, in real time, by utilizing previously surveyed TL parameters, its terminals' voltages and current readings and applying (3). Dropping the TL terminal side and phase annotations, this can be systematized by:

$$\varepsilon = V^{mea} - V^{est} \tag{9}$$

V^{mea} and V^{est} are the TL open phase voltage phasors, where the former is computed from the effectively measured data and the latter is the phasor predicted for the sound conditions. ε is the error between these two phasors, which is geometrically shown in Fig. 2.

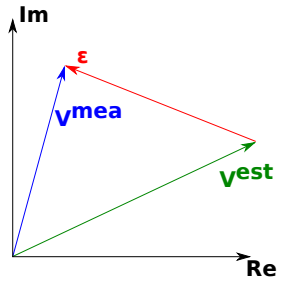

Figure 2. Geometrical interpretation of ε error.

It is important to highlight that both voltage phasors are associated with the line side of the open circuit breaker, located in the TL ending where the method will be implemented.

C. On Cross-results

A concern when developing a new method to detect an arbitrary event is the possibility of obtaining incorrect results, i.e., false positives and false negatives. These conditions would consist in the indication of a fault when the open phase is clear and the indication of a sound open phase when an LG fault is occurring, respectively. In this paper, this question was approached from an analytical perspective.

Considering an LG fault in phase A within TL terminals and that its insertion point (p) and conductance (g_f) are known, the open line voltage (V^{mea}) can also be calculated in the faulted condition by applying (3) but utilizing the proper matrix $[Q_{TL,f}]$ (4) elements, as shown in (10):

$$V^{mea,n}_{a} = -\frac{1}{q_{TL,f41}} \begin{bmatrix} q_{TL,f42} & \dots & q_{TL,f46} \end{bmatrix} \cdot \boldsymbol{b} \tag{10}$$

where $\boldsymbol{b}$ is a vector that contains the needed TL voltages and current terminal readings.

As discussed in Section II-A, the matrix $[Q_{TL,f}]$ can be generated as the sum of the original $[Q_{TL}]$ matrix with the $[\Delta Q_f]$ matrix, which denotes the TL modeling modifications motivated by the fault conductance. Thus, the terms $q_{TL,f\,ij}$ of (10) can also be split in the same manner:

$$\begin{aligned} V^{mea,n}_{a} = \frac{1}{q_{41} + \delta q_{f,41}} \Bigg\{ & -\frac{q_{41}}{q_{41}} \begin{bmatrix} q_{42} & \dots & q_{46} \end{bmatrix} \cdot \boldsymbol{b} \\ & - \frac{\delta q_{f,41}}{\delta q_{f,41}} \begin{bmatrix} \delta q_{f,42} & \dots & \delta q_{f,46} \end{bmatrix} \cdot \boldsymbol{b} \Bigg\} \end{aligned} \tag{11}$$

In (11), the terms q_{41}/q_{41} and $\delta q_{f,41}/\delta q_{f,41}$ were added to make the algebraic analysis easier. The dot product $-\frac{1}{q_{41}} \begin{bmatrix} q_{42} & \dots & q_{46} \end{bmatrix} \cdot \boldsymbol{b}$ is exactly the open terminal estimated voltage when the line is unfaulted, as expressed in (3). The second dot product $-\frac{\delta q_{f,41}}{\delta q_{f,41}} \begin{bmatrix} \delta q_{f,42} & \dots & \delta q_{f,46} \end{bmatrix} \cdot \boldsymbol{b}$ can be simplified to $-\frac{\delta q_{f,41}}{q^n_{11}} \begin{bmatrix} q^n_{12} & \dots & q^n_{16} \end{bmatrix} \cdot \boldsymbol{b}$ due to the occurrence of $\delta q_{f,ij}$ (6 to 8) in both the numerator and denominator. Moreover, $\begin{bmatrix} q^n_{12} & \dots & q^n_{16} \end{bmatrix} \cdot \boldsymbol{b}$ is almost the voltage in the fault point (Fig. 1) and is only missing the term $q^n_{11} V^n_a$. In addition, V^n_a is exactly $V^{mea,n}_a$, and thus, it is possible to rewrite the former dot product as $-\frac{\delta q_{f,41}}{q^n_{11}} \left(V^f - q^n_{11} V^{mea,n}_a \right)$, where V^f is the voltage at the fault point. Acting on the aforementioned considerations, (11) can be rewritten as:

$$\begin{aligned} V^{mea,n}_{a} = \frac{1}{q_{41} + \delta q_{f,41}} \Bigg\{ & q_{41} V^{est,n}_a \\ & + \frac{\delta q_{f,41}}{q^n_{11}} \left(q^n_{11} V^{mea,n}_a - V^f \right) \Bigg\} \end{aligned} \tag{12}$$

Replacing (12) in (9) and evaluating the algebra, it is possible to show that the error between the estimated and measured voltages can be alternatively calculated as:

$$\varepsilon = -\frac{q^m_{44}}{q_{41}} g_f V^f \tag{13}$$

Further, as the analysis has been performed considering a single frequency, the product $g_f V^f$ can be replaced by the fault current, I^f, and then:

$$\varepsilon = -\frac{q^m_{44}}{q_{41}} I^f \tag{14}$$

Therefore, (14) guarantees that, in theory, no incorrect results are possible because once the fault is eliminated, $I^f = 0$, and the error will then be zero. However, if the fault is occurring, $|I^f| > 0$, and then $|\varepsilon| > 0$.

D. Practical Considerations

Ideally, when the fault is eliminated ($g_f = 0$), it is expected that V^{mea} will tend to V^{est}, and thus, $\varepsilon \to 0$. Conversely, if the open phase still experiences a fault ($g_f > 0$), this leads to $|\varepsilon| > 0$. However, both V^{mea} and V^{est} are prone to several errors such as TL electrical parameter calculation, phasor estimation, and transduction equipment errors. Thus, ε will rarely be exactly zero when the fault is extinguished. Therefore, only checking whether ε is zero is not a practical approach.

Another possibility would be to set some limit based on the magnitude of ε, but doing so would require a significant number of previous tests to determine what value would be adequate because this variable lacks a reference.

To address this situation, an error margin that not only ensures reliability and selectivity in the fault detection but also can handle some computing errors must be considered. In doing so, the fault detection threshold is proposed as a circle centered at the end of the V^{est} phasor, with a radius length based on the percentage of the cited phasor magnitude, $r\,\%$. When ε is within the defined circle, it will be possible to determine that the fault is eliminated. This proposition is mathematically expressed in (15) and is shown in Fig. 3.

$$\underbrace{\frac{|\varepsilon|}{|V^{est}|} \times 100}_{\rho} \leq r\,\% \qquad \rho \leq r\,\% \tag{15}$$

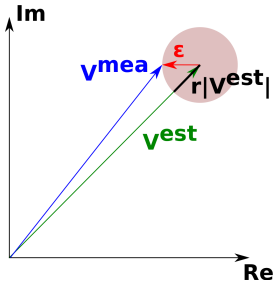

Figure 3. Geometrical interpretation of ε error - Clearance detection area.

This procedure allows some amount of discrepancy between the phasors V^{mea} and V^{est} in both magnitude and phase (θ). Its boundaries can be derived by employing (9), (15), and the cosine Law and by considering $k = {}^{|V^{mea}|}/_{|V^{est}|}$, resulting in

$$\rho^2 = 1 + k^2 - 2k\cos(\theta) \tag{16}$$

Eq. (16) permits a correlation of the magnitude ratio (k) between V^{est} and V^{mea} and its phase displacement (θ) for a given threshold $r\,\%$ that may or may not trigger the fault elimination detection. A sensitivity for k and θ for a given ρ is presented in Fig. 4.

For example, defining $r = 10$ % and if the measured and estimated voltage phasors are in phase ($\theta = 0°$), then the former may have a magnitude from 90 to 110 % of the latter (k). This is the condition in which the extrema values of ${}^{|V^{mea}|}/_{|V^{est}|}$ are found. The maximum θ occurs when V^{mea} and V^{est} have exactly the same lengths ($k = 100$ %), i.e., $\pm 5.73°$ (Fig. 5).

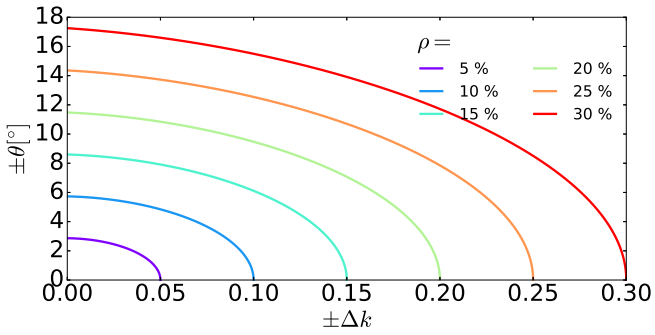

Figure 4. Correlations between k and θ for given ρ.

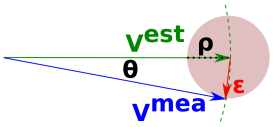

Figure 5. Geometrical interpretation of ε error - Maximum angle displacement.

In practice, the solution of (15), an inequality, should be interpreted as a logical signal. It can then be used in at least two ways to improve the SPAR reliability. The first option would be a reclosure blocking scheme based on an AND logic with CB switching signal. The second option is the advancement of open phase reclosure, once the fault is detected as eliminated and after sufficient time delay for the proper arc channel deionization.

E. Considerations in TL modeling

It is important to highlight that the four-port network must model every element effectively in operation between TL terminals and in the most reliable manner possible, i.e.:

- The electric and magnetic coupling of TLs with multiple circuits must be considered, especially if they are on the same tower;
- The transposition scheme should be represented;
- Depending on the TL length, its parameters should be corrected for the distance effect through small pi section cascading or hyperbolic correction;
- Shunt reactive compensation must be applied in the four-port network model, including the neutral grounding reactor, if existing;
- *A priori*, a series capacitor also needs to be considered; however, there are distinct scenarios implicating this equipment and its protection procedures. Therefore, each case needs to be closely analyzed.

F. Differentiation from Other Proposals

As discussed in Section I, current techniques used to detect the secondary arc extinction in the open phase for SPAR may be roughly divided into a few categories. The proposition presented in this paper falls in the open phase voltage processing

group. Indeed, it can be compared only with other methods in that same category because the very basic nature of the others groups differ. Besides to [24], in which the implementation is not clear enough, and [5], which focuses on the variation of the rms open phase voltage, all other methods [22], [23], [25], [26] have roots in the evaluation of the open phase voltage phasor position against the sound phases' voltage phasors. Those positions were studied based on a simplified capacitive network description of the TL.

What is proposed in the present document is quite different from what was surveyed in the literature. In the proposed adaptive SPAR, the open phase voltage is continuously predicted for the TL sound state, given the actual sound phases voltages and current phasors and the TL parameters. This is accomplished via the real-time simulation of the TL for the fundamental frequency, optimized for the open phase voltage. Afterwards, the predicted open phase voltage phasor (V^{est}), for the sound condition, is compared with the phasor computed from measurements (V^{mea}) - Section II-B. Additionally, it was conceived a manner to handle the errors employing a restriction region - Section II-D.

III. Proposed Method Tests

A. Steady-State Simulations

In an effort to extensively test the proposed fault detection strategy, a massive number of steady-state simulations were conducted, therein applying topological and operational variations (Section III-A1). The tests basically consisted of two steps:

1) Selecting a feasible pre-fault sound operation condition;
2) Computing ρ (Section II-D) under the open phase condition for both TL terminals in two situations:
   a) Inserted fault between TL terminals; and
   b) No inserted fault.

The test system (Fig. 6) is based on an actual Brazilian system and consists of four generators of 15 kV - 472.5 MVA, represented by its subtransient reactance (X"d = 0.1295 Ω), in series with their associated 15 kV/500 kV - 472.6 MVA step-up transformers (TF) (Table III). A 500 kV TL (Table IV) that was heavily varied, as described below, was connected to the TFs' high-voltage busbar, which is hereafter denoted Local. On the other TL ending, called Remote, a network equivalent was considered ($Z_1 = 25.1578\angle 87.3531°$ Ω), whose zero sequence parameters were also modified, as presented in the next section.

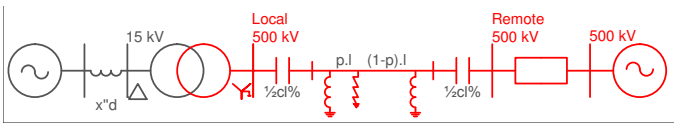

Figure 6. Steady-state single line diagram for fault detection tests.

Series and shunt compensations are shown in the system single line diagram (Fig. 6); their parameters were also varied in the manner described in Section III-A1.

Table III
Step-up Transformer Parameters.

Winding [kV]	R [Ω]	X [Ω]
500	0.795	31.338
15	0.003	0.085

Table IV
500 kV TL Parameters Calculated for 60 Hz

	R [Ω/km]	X [Ω/km]	B [μS/km]
Seq. Zero	0.4217	1.5180	2.8022
Seq. Positive/Negative	0.0134	0.2501	6.5579

The three-phase steady-state simulations were performed in the Alternative Transients Program (ATP). A specific-purpose parallel program was written in the Python language to generate ATP data cases considering the parameters and operative variations, manage the computing queue, apply the proposed methodology, and process the results.

1) Assumptions on the Variation of the Parameters: Two TL length ranges were considered, from 10 to 230 km, in steps of 24.44 km, and from 250 to 500 km, in steps of 27.78 km, without a series capacitor and for compensation levels (cl) of 50, 70 and 90 % of the TL series reactance, respectively. The series compensation were evenly split and placed in each TL terminal (Fig. 6). During the dead time, the protection scheme considered for the series capacitor was the three-phase bypass in both terminals.

Shunt compensation was only applied for $l \geq 250$ km ($cl > 0$) and was designed to supply the minimum reactive power needed to maintain the Ferranti's effect at its maximum of ${}^{1.15\,pu}/_{1.10\,pu} = 1.04\bar{5}$, as permitted in SIN by the Network Procedures (NP) [29], regarding a 500 kV voltage level. Those were four-legged reactors with a neutral reactor computed with a typical ratio of ${}^{X_0}/_{X_1} = 1.7$ [30].

Five loading levels of 0, 354.2, 708.5, 1062.75 and 1417.0 MVA were simulated, the last of which was the maximum permissible loading in the TL taken as reference. The active and reactive powers were calculated considering power factors ranging from 0.9 to 0.9889 in steps of 0.1111, leading and lagging, and 1.0. Those listed flows were imposed at the Remote terminal. The flows in the Local busbar were a consequence of those in the opposite terminal, without additional constraints.

The magnitude ratio ${}^{|Z_0|}/_{|Z_1|}$ range of the network equivalent connected to the Remote terminal was defined from 0.3 to 6.605, in steps of 1.261. Meanwhile, the angular displacement range of ${}^{Z_0}/_{Z_1}$ was -15.0 to 2.65°, in steps of 3.52°. The source for those adopted values was a preliminary short circuit study in all 500 kV busbars of SIN. The upper limit of angle displacement had to be limited to 2.65°; otherwise, $\angle Z_0$ would become greater than 90°, which would result in a non-physical negative resistance.

As a preliminary assumption, the voltage at the Remote busbar was set to 1.05 pu under sound conditions. Since the flow and voltage were imposed on this bar, all the other voltages and flows along the test system, especially in infinite

sources to be adjusted in the ATP data case, could be promptly calculated.

The feasibility of each resulting configuration based on the combinations of the aforementioned parameter variations under the sound condition was checked based on their voltage magnitudes (v) in the machine terminals, the Local busbar and the line-side of the series capacitors (when present); they should comply with the following pu limits, respectively: $0.95 \leq v \leq 1.05$ pu, $1.00 \leq v \leq 1.10$ pu and $v \leq 1.10$ pu. Otherwise, they were rejected and not considered to be studied.

The cases that had shown themselves to be feasible were then processed in ATP, with one open phase under sound and faulted conditions. Under the former condition, the fault resistance (r_f) was varied to 10^{-3}, 10^{1}, 10^{2}, $3{\cdot}10^{2}$ and 10^{3} Ω, as well as its placement along TL (p) in the range of 0.1 to 99.9 %, in steps of 5.25%.

The threshold adopted to consider whether the system was faulted was the same as for the example given in Section II-D: $r = 10$ %.

If all the parameter combinations were feasible, there would have been more than 9.5 million simulations to be processed. However, when performing the system integrity test, some of them were disregarded due to operational voltage constraints, resulting in a smaller number of actual simulated cases.

B. Time-Domain Simulations

Preliminary time-domain simulations were performed to verify the proposed method using ATP as well. The SPAR was simulated utilizing the most critical case topology and operation point selected from the steady-state analysis. The switchings were commanded as follows:

1) LG fault inception: 25 ms;
2) Opening of the phase closer to the fault inception point: 75 ms;
3) Opening of the phase farther to the fault inception point: 95 ms;
4) Fault elimination: 225 ms;
5) Reclosing of the first phase to open: 575 ms; and
6) Reclosing of the second phase to open: 595 ms.

The voltages and current phasors were estimated applying a method based on a conventional Discrete Fourier Transform (DFT) [31]. The window time length was considered as one period of a full cycle, or FCDFT, with 8 samples per window.

IV. Results and Analysis

A. Steady-State Simulations

The results of the application of the proposed methodology for all the generated steady-state simulation cases, as described in the previous section, are summarized in Figs. 7 and 8; they consist of the computed ρ (15) for both TL terminals and either conditions of the open phase for SPAR, sound ($\times$ marker) and faulted ($\bullet$ marker). The dashed magenta line represents the edge of the clearance detection area (Section II-D), where the values above this line are understood as a faulted condition by the proposed method, whereas the values below the refereed line, within the shaded area, regards to the sound condition.

Table V
Summary of effectively processed cases.

Series comp. level [%]	Number of cases	Total time [s]
0	1,577,500	24,466
50	1,252,500	17,710
70	1,550,000	20,763
90	1,625,000	22,671

The effective number of processed simulations and their time durations are presented in Table V.

The first and most important piece of information that can be extracted from the results is that the employed methodology was capable of successfully distinguishing between sound and faulted conditions of the TL, open phase for the SPAR maneuver, in every simulation. This is depicted by the lack of $\rho > 10$ % when the TL is sound and $\rho < 10$ % for the faulted open phase.

It can be seen that ρ is not exactly zero in the unfaulted condition, as the theory would indicate (Section II-A). This situation is explained by the different TL models used in the methodology, the four-port network, and in ATP, Bergeron's model. The TL modeling error accumulates as the line becomes longer (l), as can be noted by evaluating the results where l varies from 10 to 230 km (no series compensation - purple to red - Figs. 7-a and 8-a), with even larger deviations from 250 to 500 km (series compensated lines - purple to red - Figs. 7-b,c,d and 8-b,c,d). The error for the longest uncompensated line (red - $l = 230$ km) is numerically close to the shortest series compensated line (purple - $l = 250$ km). Nonetheless, there is sufficient margin, even for TLs of 500 km, for correctly identifying whether the open phase is sound.

Under the sound condition, the error bar extrema are close to the mean ρ value, indicating an insignificant dependence of this variable considering all the parameter variations, except for the TL length (l). That variable (l) clearly showed a non-linearly proportional interference in ρ.

The opposite condition is found when the open phase is faulted, once the error bars showed meaningful dispersion over the mean value (Fig. 9). This shows that the other parameters, aside from p and l, interfere significantly in ρ. When the error bar superior edge diverges from the mean value, the method is less likely to produce an incorrect result. Conversely, when the inferior edge deviates from the mean value, the method is more likely to indicate a sound open phase, even though it is still faulted. Nevertheless, none of the last conditions were remotely found. The following set of parameters resulted in the smaller ρ of 54.876 %:

- Terminal: Local (p = 0 %);
- TL length (l): 230 km;
- Compensation level (cl): 0 %;
- Three-phase power flow at the Remote terminal: 1417 MVA @ pf = 1;
- Fault location along TL (p): 63.132 %;
- Fault resistance (r_f): 1,000 Ω;
- Magnitude ratio of $|Z_0|/|Z_1|$: 0.300; and

This article has been accepted for publication in a future issue of this journal, but has not been fully edited. Content may change prior to final publication. Citation information: DOI 10.1109/TPWRD.2018.2855105, IEEE Transactions on Power Delivery

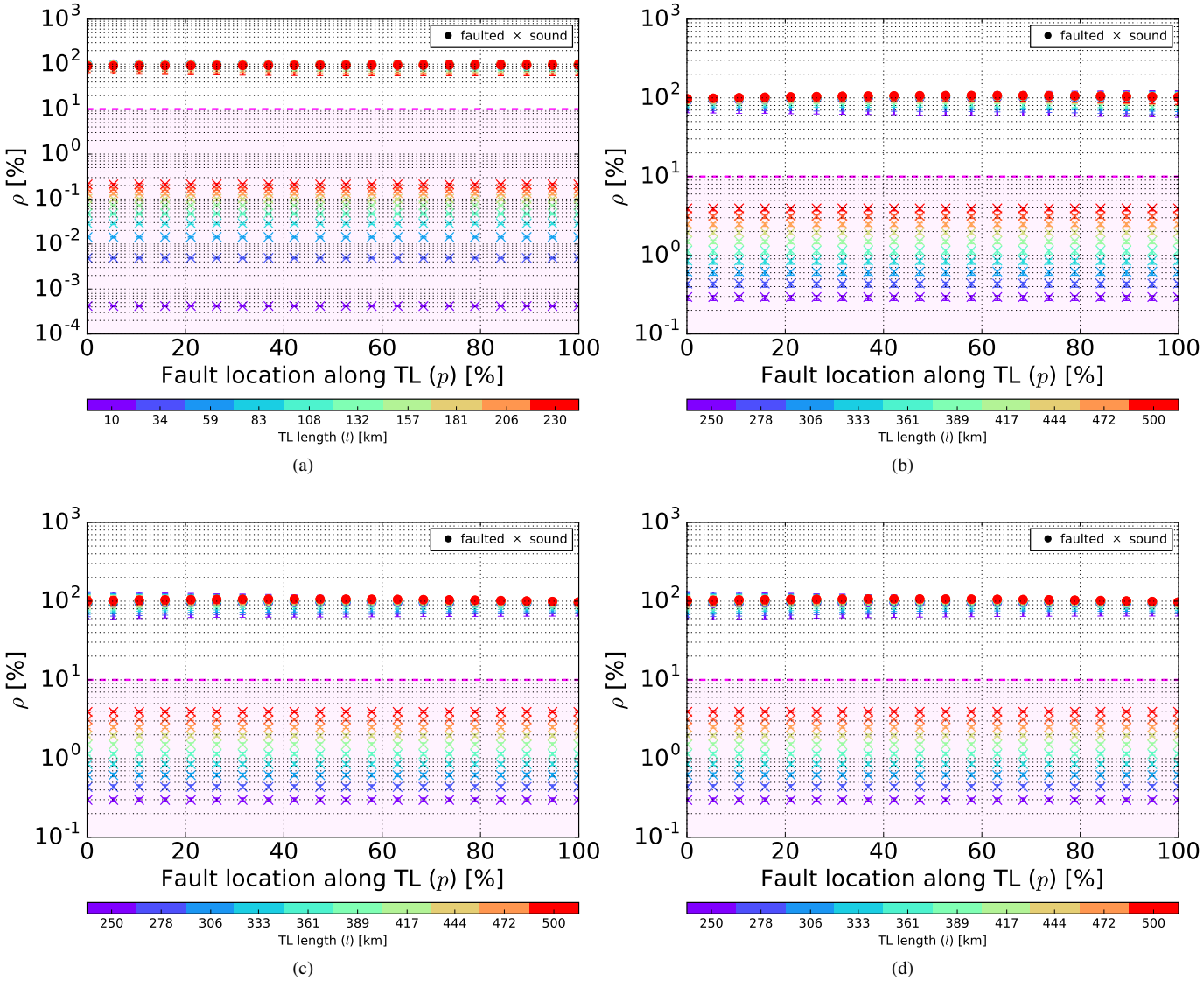

Figure 7. Steady-state parametric variation results for series compensation levels of (a) 0 %, (b) 50 %, (c) 70 % and (d) 90 % - Local terminal (p=0 %) - The superior and inferior error bar edges are the maximum and minimum values found. The • and × markers represent the mean values. The shaded area represents the clearance detection region.

- Displacement angle of $^{Z_0}/_{Z_1}$: 2.647°.

As listed above, the minimum ρ value found occurred for the maximum resistance value considered. This is an expected result because the error magnitude is directly proportional to the fault current (Section II-C), which in turn is inversely proportional to the fault resistance (Fig. 9).

In EHV and UHV transmission systems, a fault resistance of 1,000 Ω is an extremely unusual high value but was used for this paper in an attempt to drive the proposed method to its limits; even then, this method was still able to properly differentiate sound and fault conditions. If a more reasonable smaller fault resistance was considered, e.g., one no greater than 300 Ω [24], no ρ smaller than 80 % would be found.

The application of the proposed methodology correctly identified the actual open phase condition from both terminals in an independent manner. This shows that communication between the terminals of the TL is not needed. Additionally, the method may be implemented in only one of the TL terminals, preferably in the terminal that is the SPAR leader. These features are interesting since they reduce not only the costs of the proposed strategy implementation but also its complexity.

B. Time-Domain Simulations

The most critical scenario found in the steady-state analysis was used as a reference topology and operation point for time-domain simulations. As it was previously verified that the detection can be independently realized from any terminal, the proposed method was tested only for the Local terminal, which presented the smaller ρ for the faulted condition. The results are presented in Table VI and Fig. 10.

First, it is remarkable that the effects of the LG fault in the line-to-ground voltages were not easily seen, especially in the faulted phase A, at the instant of its inception and a few cycles

This article has been accepted for publication in a future issue of this journal, but has not been fully edited. Content may change prior to final publication. Citation information: DOI 10.1109/TPWRD.2018.2855105, IEEE Transactions on Power Delivery

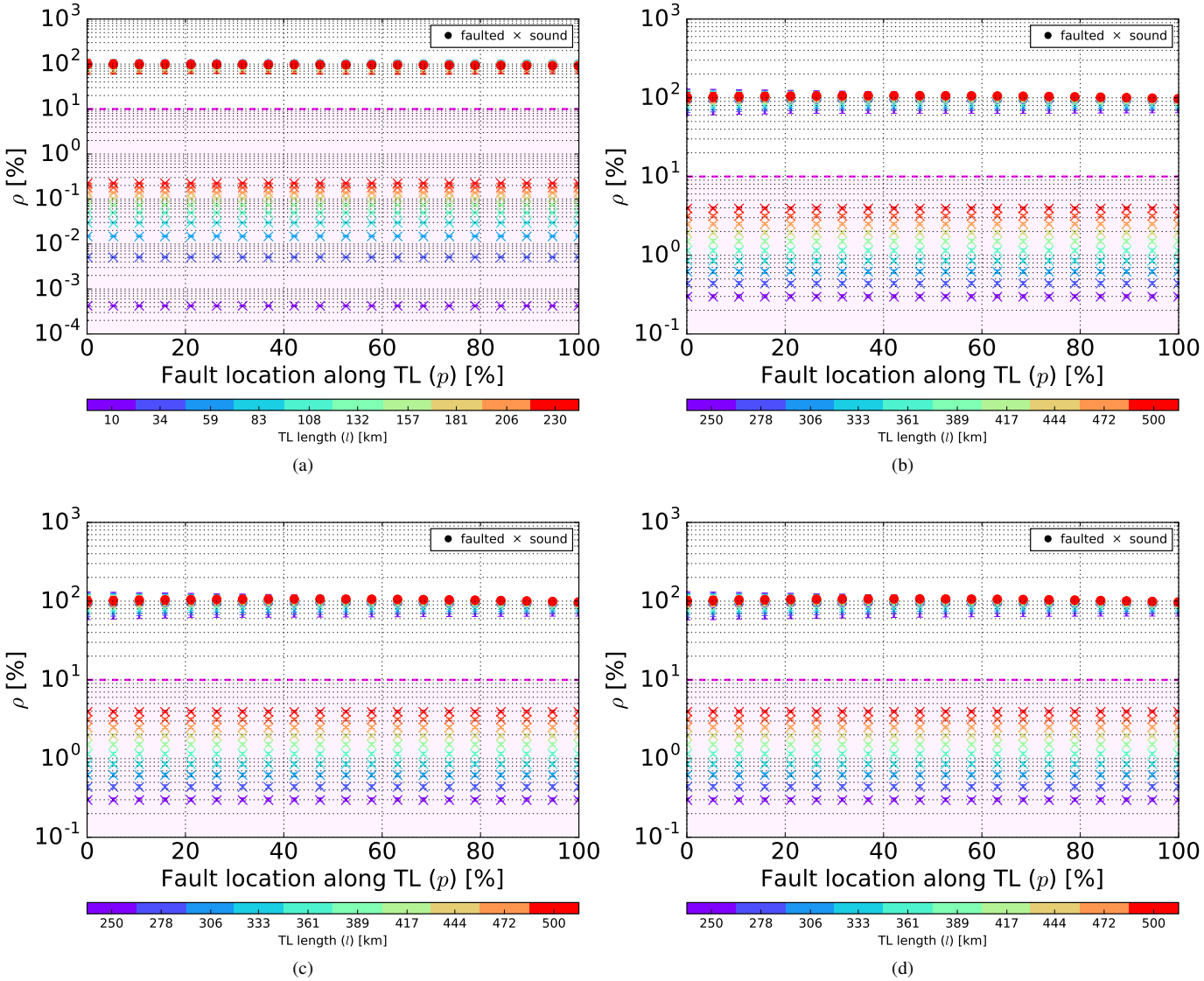

Figure 8. Steady-state parametric variation results for series compensation levels of (a) 0 %, (b) 50 %, (c) 70 % and (d) 90 % - Remote terminal (p=100 %) - The superior and inferior error bar edges are the maximum and minimum values found. The • and × markers represent the mean values. The shaded area represents the clearance detection region.

Table VI
SPAR SIMULATION EVENTS.

Event	Time [ms]
LG fault inception - phase A	25.05
First pole to open (Remote)	79.21
Second pole to open (Local)	100.35
Fault elimination	227.22
Detection of fault elimination	238.92
First pole to close (Remote)	575.02
Second pole to close (Local)	595.04

later. This is because of the high fault resistance (r_f) value adopted.

Before the opening of the faulted phase, ρ remains above 400 %. Afterwards, its value drops to 54.9 %, which is very close to the value of 54.876 % obtained in the steady-state analysis. It is important to highlight that in the time-domain analysis, the error from the FCDFT phasor estimation was considered. When the fault is eliminated, ρ crosses the threshold line of 10 %, achieving values on the order of 0.05 %, and then correctly signals that the open phase is in the sound condition. The last event of the simulation is the reclosing of the line, and ρ is then driven again to values higher than 400 %.

It can be noted that even though V^{mea} and V^{est} have similar magnitudes (Fig. 10-c) under the open phase faulted condition, ρ still has noticeably higher values than the threshold of 10 %. This condition occurs because the proposed method utilizes a full phasor comparison, both in magnitude and phase. As can be seen in Fig. 10-d, in the aforementioned condition, there is a phase displacement of 30° between V^{mea} and V^{est}, therefore ensuring the correct fault presence indication at that moment.

ρ has shown a large numerical gap in-between each of the TL's possible operating conditions during SPAR, namely,

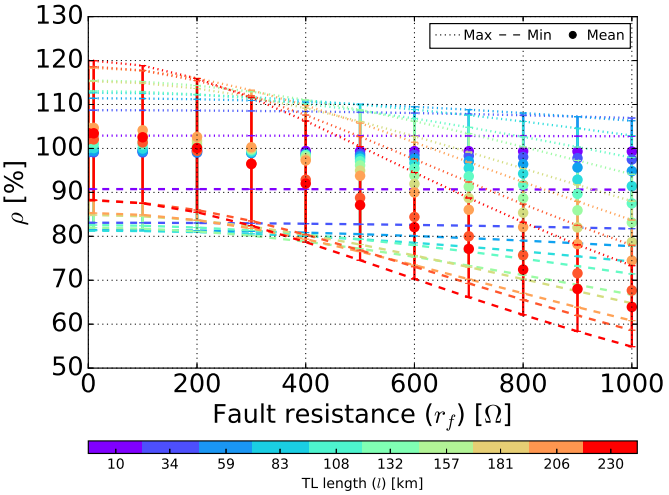

Figure 9. Steady-state parametric variation results for series compensation level of 0 % for faulted condition - Local Terminal (p=0 %) - Expanded fault resistance range.

three-phase operation under sound and faulted conditions and one open phase under faulted and sound conditions, the last being the condition that presented the most reduced ρ values. This shows that as envisioned theoretically (Section II-C) and exhaustively tested in steady-state simulations, incorrect results are by no means expected, even when employing the unusual fault resistance of 1,000 Ω. In addition, it is possible to utilize the referenced large gap to fine tune the ρ threshold ($r\%$). Reducing the clearance detection area would improve the proposed method selectivity and reliability, whereas increasing it would make the proposed method faster and better in addressing possible phasor estimation and parameter errors.

The proposed method needed 11.70 ms to detect the TL clearance, which corresponds to 0.70 of the period of a 60 Hz synchronous sine wave. Thus, it can be considered fast enough to be implemented along the SPAR dead time.

V. Conclusions

This paper has presented a new methodology for fault detection in open phase during a SPAR maneuver. It is based on the sound voltage phasor estimation for the TL open phase during dead time and comparison against the truly measured one. The main focus was to disclose its fundamental concepts and mathematical background.

A massive number of steady-state tests were performed, therein varying several topological parameters and operational conditions. No incorrect results were obtained, as theoretically expected.

Moreover, a preliminary time-domain simulation was performed utilizing the most critical case found in the steady-state analysis, which confirmed that the proposed method not only was capable of identifying the open phase clearance but also did so in less than one cycle.

Considering the promising results obtained, the authors are encouraged to push the research further by testing the proposed methodology with more time-domain simulations, dynamic arc models, oscillographic records obtained in field measurements,

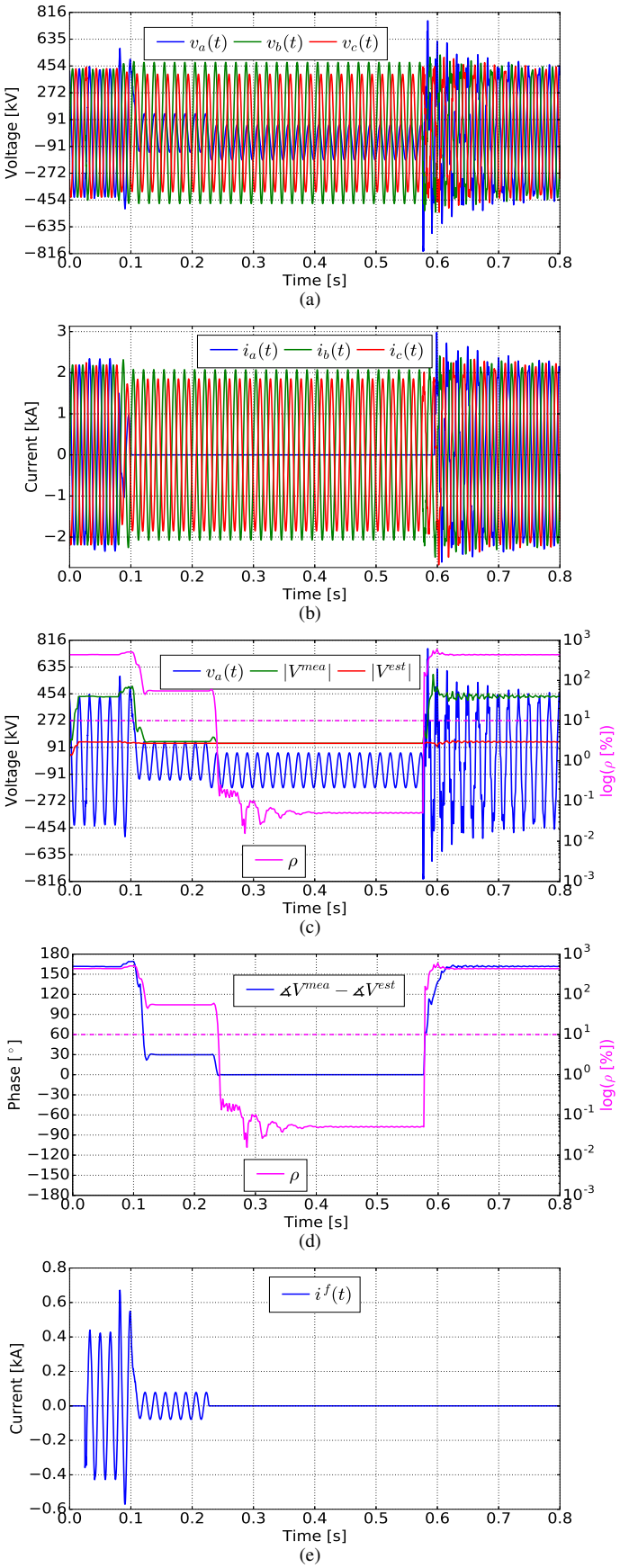

Figure 10. Voltage (a) and current (b) waveforms, open phase waveform, phasors V^{mea} and V^{est} magnitudes, and ρ performance (c), angular displacement between the open phase voltages phasors measured and estimated (d) for the Local terminal (p=0 %). Fault current (e).

and real-time simulations including industrial-grade hardware in the loop.

ACKNOWLEDGMENT

The authors would like to thank Professor Felippe Beaklini, who is with the Physics Institute of the University of Brasília, for providing a higher processing capacity computer that allowed the massive steady-state simulations and analysis of their results.

REFERENCES

[1] W. Humpage and B. Stott, "Effect of autoreclosing circuit breakers on transient stability in e.h.v. transmission systems," *Proceedings of the Institution of Electrical Engineers*, vol. 111, no. 7, pp. 1287–1298, 1964.

[2] A. J. Gonzalez, G. Kung, C. Raczkowski, C. Taylor, and D. Thonn, "Effects of single-and three-pole switching and high-speed reclosing on turbine-generator shafts and blades," *IEEE Power Engineering Review*, vol. PER-4, no. 11, 1984.

[3] M. of the IEEE Power System Relaying Committee Working Group, "Single phase tripping and auto reclosing of transmission lines-IEEE committee report," *IEEE Transactions on Power Delivery*, vol. 7, no. 1, pp. 182–192, 1992.

[4] C. Ferreira, J. Pinto, and F. Barbosa, "Effect of the single and three phase switching in the transient stability of an electric power system using the extended equal area criterion," in *Electrotechnical Conference, 1998. MELECON 98., 9th Mediterranean*, vol. 2, 1998, pp. 950–953.

[5] S.-P. Ahn, C.-H. Kim, R. K. Aggarwal, and A. T. Johns, "An alternative approach to adaptive single pole auto-reclosing in high voltage transmission systems based on variable dead time control," *IEEE Transactions on Power Delivery*, vol. 16, no. 4, pp. 676–686, 2001.

[6] G. Samorodov, S. Zilberman, and E. Krasilnikov, "Application of Half-Wave Transmission systems for Power delivery over extra long distances 2000-4000 km," in *IEEE Electrical Power and Energy Conference*. Winnipeg: IEEE, 2011, pp. 351–356.

[7] ONS, "Statistical analysis of forced tripping for the year 2016 - Transmission lines (in Portuguese)," Tech. Rep., 2017.

[8] W. Elmore, *Protective Relaying: Theory and Applications*, 2nd ed., 2004.

[9] R. G. NORDIC, "Nordic grid disturbance statistics 2013," ENTSOE, Tech. Rep., 2014.

[10] Z. Bo, R. Aggarwal, A. Johns, B. Zhang, and Y. Ge, "New concept in transmission line reclosure using high-frequency fault transients," *IEE proceedings-generation, transmission and distribution*, vol. 144, no. 4, pp. 351–356, 1997.

[11] Z. Bo, R. Aggarwal, and A. Johns, "A novel technique to distinguish between transient and permanent faults based on the detection of current transients," vol. 1, pp. 216–220, 1997.

[12] M. H. Golshan and N. Golbon, "Detecting secondary arc extinction time by analyzing low frequency components of faulted phase voltage or sound phase current waveforms," *Electrical Engineering*, vol. 88, no. 2, pp. 141–148, 2006.

[13] Z. M. Radojević, "Numerical algorithm for adaptive single pole autoreclosure based on determining the secondary arc extinction time," *Electric Power Components and Systems*, vol. 34, no. 7, pp. 739–745, 2006.

[14] Z. M. Radojević and J.-R. Shin, "New digital algorithm for adaptive reclosing based on the calculation of the faulted phase voltage total harmonic distortion factor," *IEEE Transactions on Power Delivery*, vol. 22, no. 1, pp. 37–41, 2007.

[15] M. Jannati, B. Vahidi, S. Hosseinian, and H. Baghaee, "A new adaptive single phase auto-reclosure scheme for EHV transmission lines," in *Power System Conference, 2008. MEPCON 2008. 12th International Middle-East*, 2008, pp. 203–207.

[16] A. Montanari, M. Tavares, and C. Portela, "Adaptative single-phase autoreclosing based on secondary arc voltage harmonic signature parameters," in *IPST, Kyoto, Japan*, 2009.

[17] O. Dias and M. C. Tavares, "Comparison between traditional single-phase auto reclosing and adaptive technique based on harmonic content measurement," *IET Generation, Transmission & Distribution*, vol. 11, no. 4, pp. 905–914, 2017.

[18] G. Ban, L. Prikler, and G. Banfai, "Testing ehv secondary arcs," in *Power Tech Proceedings, 2001 IEEE Porto*, vol. 4. IEEE, 2001, pp. 6–pp.

[19] N. I. Elkalashy, H. A. Darwish, A.-M. I. Taalab, and M. A. Izzularab, "An adaptive single pole autoreclosure based on zero sequence power," *Electric Power Systems Research*, vol. 77, no. 5, pp. 438–446, 2007.

[20] D. Fitton, R. Dunn, R. Aggarwal, A. Johns, and A. Bennett, "Design and implementation of an adapative single pole autoreclosure technique for transmission lines using artificial neural networks," *IEEE Transactions on Power Delivery*, vol. 11, no. 2, pp. 748–756, 1996.

[21] Y.-H. Lin, C.-W. Liu, and C.-S. Chen, "A new pmu-based fault detection/location technique for transmission lines with consideration of arcing fault discrimination-part i: theory and algorithms," *IEEE Transactions on power delivery*, vol. 19, no. 4, pp. 1587–1593, 2004.

[22] J. Giesbrecht, D. S. Ouellette, and C. F. Henville, "Secondary arc extinction and detection real and simulated," in *Developments in Power System Protection, 2008. DPSP 2008. IET 9th International Conference on*. IET, 2008, pp. 138–143.

[23] A. Guzmán, J. Mooney, G. Benmouyal, N. Fischer, and B. Kasztenny, "Transmission line protection system for increasing power system requirements," in *Proc. Int Modern Electric Power Systems (MEPS) Symp*, Sep. 2010, pp. 1–11.

[24] Y. Yang, Y. Li, and G. Pradeep, "Voltage based method for fault identification in a transmission line and apparatus thereof," Mar. 17 2011, uS Patent App. 13/982,297.

[25] M. Zadeh, I. Voloh, M. Kanabar, and Y. Xue, "An adaptive hv transmission lines reclosing based on voltage pattern in the complex plane," in *2012 65th Annual Conference for Protective Relay Engineers*. IEEE, 2012, pp. 85–95.

[26] M. Nagpal, S. H. Manuel, B. E. Bell, R. P. Barone, C. Henville, and D. Ghangass, "Field verification of secondary arc extinction logic," *IEEE Transactions on Power Delivery*, vol. 31, no. 4, pp. 1864–1872, Aug. 2016.

[27] R. D. Fuchs, *Electric Energy Transmission (in Portuguese)*, 1977, vol. 1.

[28] W. Bowman and J. McNamee, "Development of equivalent pi and t matrix circuits for long untransposed transmission lines," *IEEE transactions on Power Apparatus and Systems*, vol. 83, no. 6, pp. 625–632, 1964.

[29] ONS, "Guideline and criteria for electrical studies - submodule 23.3 (in Portuguese)," Tech. Rep., 2011.

[30] P. Mestas and M. Tavares, "Neutral reactor optimization in order to reduce arc extinction time during three-phase tripping," in *IPST, Cavtat, Croatia*, 2015.

[31] K. M. Silva and F. A. O. Nascimento, "Modified DFT-based phasor estimation algorithms for numerical relaying applications," *IEEE Transactions on Power Delivery*, vol. PP, no. 99, p. 1, 2017.

Leonardo M. N. de Mattos was born in Rio de Janeiro, Brazil, in 1987. He received his Electrical Engineering degree from the University of Brasília (UnB/2012) and his M.Sc. degree from the University of Campinas (UNICAMP/2017). He is presently working as a self-employed consultant in power systems operation and planning electrical studies. His research interests include power systems analysis, electromagnetic transients and high-performance computing.

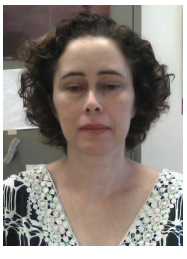

M. C. Tavares (SM 2008) is currently an associate professor at the University of Campinas, where she has been since 2002. She received degrees in electrical engineering from the Federal University of Rio de Janeiro (UFRJ) in Brazil (1984), her M.Sc. (1991) from the same university, and her D.Sc. (1998) from UNICAMP. She has provided consultation for engineering firms, and her main interests are power system analysis, electromagnetic transients, arc modeling and very long distance transmission systems.

Aniela M. P. Mendes was born in Brasília, Brazil. She received a degree in electrical engineering from the University of Brasília (UnB/2006) and her M.Sc. degree from the University of Campinas (UNICAMP/2017). Since 2006, she has been working at Eletrobras Eletronorte on power system operation planning studies. Her main fields of interest are power systems, electromagnetic and electromechanical transients, and load flow.